THE JOURNAL OF PHYSICAL CHEMISTRY C

Article

Cite This: J. Phys. Chem. C 2018, 122, 7676−7684

pubs.acs.org/JPCC

Nanoconfinement-Induced Phase Segregation of Binary Benzene−Cyclohexane Solutions within a Chemically Inert Matrix

Kathryn L. Krycka,[†,*] Joseph A. Dura,[†] Luther J. Langston, II,[‡] and Christopher M. Burba[‡,*]

[†]NIST Center for Neutron Research, National Institute of Standards and Technology, Gaithersburg, Maryland 20899, United States

[‡]Department of Natural Sciences, Northeastern State University, Tahlequah, Oklahoma 74464, United States

Supporting Information

ABSTRACT: Binary solutions provide a fertile arena to probe intermolecular and molecular/surface interactions under nanoconfinement. Here, the phase segregation of a solution comprising 0.80 mol fraction benzene and 0.20 mol fraction cyclohexane confined within SiO_2 nanopores was evaluated using small-angle neutron scattering with hydrogen−deuterium contrast matching. It is demonstrated that benzene and cyclohexane are fully miscible at 303 K (30 °C), yet they unambiguously phase segregate by 153 K (−120 °C), which is below their respective freezing points and below the cubic-to-monoclinic phase transition of cyclohexane. Specifically, the cyclohexane and benzene separate into a core|shell morphology with cyclohexane concentrated toward the nanopore centers. Additionally, pure benzene is shown to form a frozen core of bulk density with a thin shell of slightly reduced density immediately adjacent to the SiO_2 nanopore wall at 153 K. Because the SiO_2 matrix is chemically inert to cyclohexane and benzene, the observed radially dependent phase segregation is strong evidence for the effects of confinement alone, with minimal host−wall attraction.

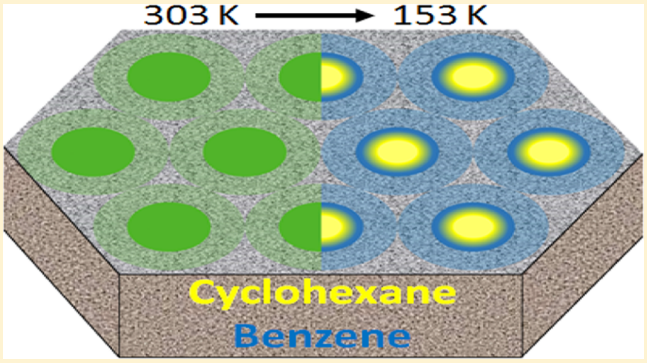

INTRODUCTION

Liquids confined within mesoporous materials often exhibit unusual properties, including reduced melting points, slowed molecular dynamics, and increased densities compared to that of unconfined liquids. The general consensus is that these effects arise from molecular interactions between the liquid and walls of the confinement host. In pores with relatively large diameters, liquids often form crystalline solids with a one or two monolayer thick nonfreezable interfacial layer when the temperature is lower than the melting point of the confined liquid. In the small pore regime, however, crystallization may be completely suppressed.[1] The physics of confinement-induced melting point depression is typically described by the Gibbs−Thomson equation, for which the change in the melting point of a confined liquid is inversely proportional to the radius of the pore. This approach adequately describes thermal properties for a large number of liquids that form strong intermolecular interactions with the wall, such as the archetypal example of the water−mesoporous SiO_2 system. There are many examples, however, where the equation is deficient.[2−7] Thus, understanding confinement-induced changes for liquids that lack strong interactions with the host−wall, such as those with only van der Waals interactions like benzene[4,6,8−10] and cyclohexane,[5] is especially important.

Whereas the phase behavior of confined, single-component liquids is fairly well understood, the properties of confined solutions remains comparatively unexplored. From both a fundamental research point of view and the potential applications involving confined liquids, it is vital to have a clear picture of how surface interactions influence the behavior of solutions. In particular, it is not known whether or not the nonfreezable surface layer retains the same overall solution composition when confined solutions are frozen. Therefore, we have chosen to focus on a binary solution of cyclohexane and benzene to quantitatively assess the composition and morphology of the nonfreezable surface layer under confinement and in the absence of appreciable solution−wall attraction.

Benzene and cyclohexane form nonideal solutions at room temperature with positive deviations from Raoult's law.[11] The solid−liquid phase diagram has a single eutectic point at 234 K.[12−15] Consequently, a frozen mixture of benzene and cyclohexane will contain a mixture of benzene and cyclohexane crystallites, with the relative amounts of each being governed by the overall sample composition. Although the compounds are hydrophobic, both solvents wet quartz surfaces, having sessile drop contact angles of ∼10°.[16] Moreover, the two compounds experience reduced melting point temperatures when confined within mesoporous silica, and the cubic-to-monoclinic solid phase transition for cyclohexane (186 K) also occurs at reduced

Received: November 17, 2017
Revised: March 8, 2018
Published: March 20, 2018

DOI: 10.1021/acs.jpcc.7b11365
J. Phys. Chem. C 2018, 122, 7676−7684

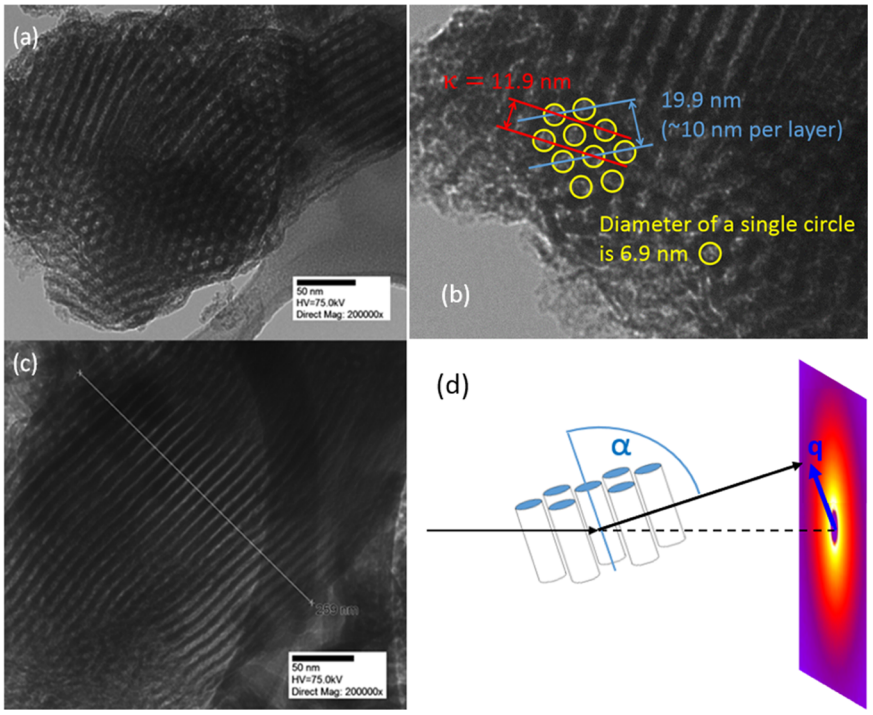

Figure 1. (a, b) TEM images indicate that the pores are hexagonally close-packed. (c) TEM cross section of the pores indicates that they are relatively straight and thin walled. (d) SANS setup (not drawn to scale) shows how an ensemble average of packed pores over all orientations is probed in terms of angle α.

temperatures under confinement (about 173 K).[5] There is indirect evidence of a distinctive near-wall region in frozen benzene, whose thickness, density, and ordering characteristics are under debate.[7,9,10,17,18]

Small-angle neutron scattering (SANS) is uniquely poised to address questions about how solutions interact with the pore walls of a mesoporous host.[19] In particular, benzene, cyclohexane, and mesoporous silica have different scattering length densities (SLDs) that will enable contrast matching of the solution SLD to that of silica with protonated and deuterated versions of the solvents. This will provide a powerful set of tools for examining these solutions under confinement. Contrast matching a solution to the SLD of silica at room temperature will minimize the intensities of the Bragg peaks associated with the mesopore lattice. If the nonfreezable layer retains the overall solution composition upon freezing, the average SLD—apart from small density changes—should remain contrast matched to silica. Conversely, compositional variation of the nonfreezable layer will break the contrast matching between the solution and the pore walls, giving rise to Bragg peaks of measurable intensity.

SANS has previously been used to examine the interaction of benzene in confined silica samples. Early work by Ramsay and Hoinkis[20] used SANS to explore the adsorption of deuterated benzene (DB) on porous silica gels, whereas Xia et al.[17] used neutron scattering to investigate the solid−liquid phase transition of benzene confined within MCM-41 (2.4 nm $\leq d \leq$ 3.6 nm) and SBA-15 mesoporous silicas (4.7 nm $\leq d \leq$ 14 nm). Static structure factors obtained from neutron diffraction of the frozen samples (T = 70 K) revealed crystallization of benzene within the larger-sized pores, but benzene vitrified in smaller pores to form an amorphous solid. Lin et al. applied contrast matching to examine liquid−liquid phase separation in the H_2O−2,6-lutidine system.[21] Hellweg et al.[22] and Schemmel et al.[23] also used SANS to demonstrate the demixing of confined binary solutions of iso-butyric acid and D_2O below the upper critical solution temperature. In a similar set of SANS experiments, Hamid and co-workers[24] established microphase separation of iso-butanol and toluene upon confinement. Iso-butanol forms hydrogen bonds with Si−O and Si−OH groups along the pore wall−solution interface; thus, this component accumulates along the pore wall to produce an iso-butanol-rich shell with a toluene-rich core at room temperature. All of these systems differ from our work in that in those cases, one or both of the components is capable of hydrogen bonding with silica. Neither benzene nor cyclohexane is able to form hydrogen bonds; thus, we do not anticipate either compound to have a particularly strong affinity for the pore wall.

EXPERIMENTAL METHODS

Our sample involves a mesoporous silica (SiO_2) matrix of hexagonally packed cylindrical pores purchased from Sigma-Aldrich. Characterization of the mesoporous silica is provided in the Supporting Information. Notably, it appears to contain a large fraction of voids by volume, which are solution penetrable. Differential scanning calorimetry (Mettler DSC 1) was used to identify thermal transitions from mesoporous silica flooded with benzene−cyclohexane solution. DSC samples consist of 4.3 ± 0.6 mg mesoporous silica mixed with 24.9 ± 3.3 mg solution, yielding a silica mass fraction of 14.9 ± 2.0%. Samples were then hermetically sealed in 40 μL aluminum crucibles, and thermal transitions were recorded at a 10 K min^{-1} scan rate under a dry nitrogen atmosphere.

SANS patterns were collected at the NIST Center for Neutron Research beam line NGB 30 m SANS. Samples consisted of mesoporous silica packed into a 1.0 mm-thick sample holder with quartz windows. The sample cells were filled with mesoporous silica and either flooded with excess

DOI: 10.1021/acs.jpcc.7b11365
J. Phys. Chem. C 2018, 122, 7676−7684

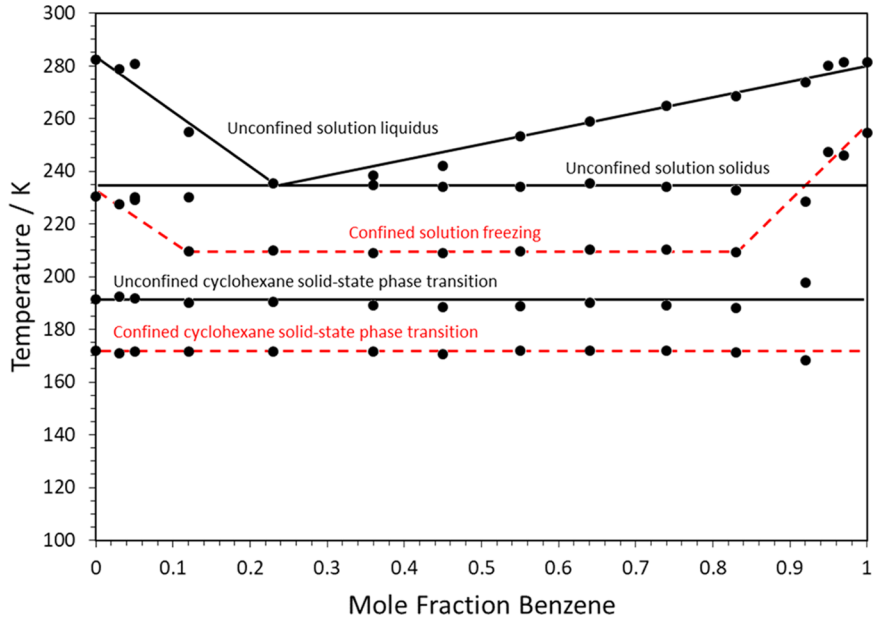

Figure 2. Phase transition temperatures for benzene−cyclohexane solutions in contact with mesoporous silica obtained from DSC (10 K min^{-1} scan rate). Transitions assigned to the confined solutions are marked with a dashed red line.

benzene−cyclohexane solution (0.80 mol fraction benzene), flooded with pure benzene, or left open and baked, before sealing. The incident neutron wavelength was 0.60 nm with an 11% full-width half maximum wavelength spread. Data were collected with a two-dimensional detector at sample-to-detector distances of 13.035, 4.535, and 1.865 m, with the detector offset by 25 cm in a direction perpendicular to the incident neutron beam at 1.865 m to obtain the highest momentum transfer. The data from the three detector distances were combined and placed onto an absolute scale using in-house software.[25]

RESULTS AND DISCUSSION

Description of the Mesoporous Silica. As described above, the pores of the mesoporous silica are either unfilled (open) or filled with deuterated benzene (DB), 0.80 mol fraction deuterated benzene and 0.20 mol fraction deuterated cyclohexane (DBDC), or 0.80 deuterated benzene and 0.20 protonated cyclohexane by mole fraction (DBPC). This particular composition of benzene is selected such that the DBPC sample will be approximately contrast matched to the SiO_2 host matrix as viewed by neutron scattering when the solution is fully miscible. The pores are hexagonally close-packed, Figure 1, as indicated by transmission electron microscopy (TEM). The pore-to-pore distance, κ, shows some variation between 11.5 nm (blue marker in Figure 1b) and 11.9 nm (red marker in Figure 1b). X-ray scattering places the primary interparticle peak at 0.057 $Å^{-1}$ (see the Supporting Information). In a hexagonally close-packed system, this would correspond to the $\sqrt{3}\kappa/2$ reflection, yielding κ = 12.7 nm. A TEM image from a slice along the pore walls, Figure 1c, shows that the pores are relatively straight and thin walled deep within the sample interior. Comparison with the surface TEM image in Figure 1b suggests that the pores narrow toward the surface. N_2 physisorption data indicates that the internal diameter of the pores is about 9 nm, and Hg porisometry data indicates that the mesoporous silica is highly porous.

Phase Behavior of Confined Benzene−Cyclohexane Solutions. Thermal transitions for benzene−cyclohexane solutions in the presence of mesoporous silica are presented in Figure 2. The pure benzene sample exhibits two phase changes. The higher temperature phase transition is assigned to the fusion of unconfined benzene present in an external liquid reservoir. The lower temperature phase transition is attributed to the fusion of benzene that is confined within the silica mesopores. Four phase transitions are observed for the sample containing pure cyclohexane in contact with the mesoporous silica. Similar to pure benzene samples, the fusion of confined cyclohexane occurs at lower temperatures than that of unconfined cyclohexane. We also observed a reduction in the cubic-to-monoclinic solid-state phase transition temperature when cyclohexane is constricted within the mesoporous silica (190−171 K); this finding is similar to other reports concerning the phase behavior of confined cyclohexane.[5,8,14,17,26] Continuing to observe the 171 K phase transition, regardless of solution composition, provides compelling evidence that benzene−cyclohexane solutions phase separate within the pores at low temperatures.

The phase transitions for unconfined solutions match the known phase diagram of benzene and cyclohexane.[12] It should be noted, however, that the phase behavior of solutions containing deuterated components may be slightly different from that of the protonated analogues. Confined solutions show relatively constant melting points at ∼210 K over a broad range of solution compositions (approximately 0.1−0.8 mol fraction benzene). Our samples consist of confined benzene−cyclohexane solution in contact with an external reservoir of unconfined solution. When the sample temperature falls below the freezing point of the unconfined solution, the majority component crystallizes in the external reservoir and the unconfined solution composition will be driven toward the eutectic composition. It is plausible that confined solutions undergo mass exchange with the external reservoir and also adopt the eutectic composition. Hence, the 210 K phase transition may originate from the fusion of confined solutions that have the eutectic composition. These observations are similar to the findings of Meissner et al.,[27] wherein the melting

DOI: 10.1021/acs.jpcc.7b11365
J. Phys. Chem. C 2018, 122, 7676−7684

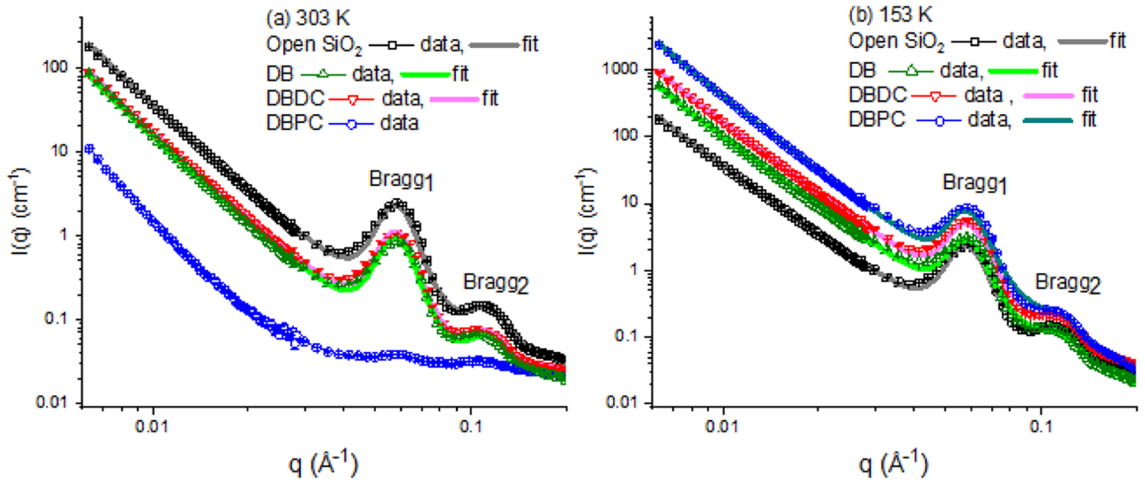

Figure 3. (a) SANS scattering on absolute scale at 303 K (a) and 153 K (b). Except for the contrast matched DBDC at 300 K, the data are each fit with a Porod slope plus three Lorentzians at (0.058, 0.112, and 0.18 Å^{-1}) of variable amplitudes. Errors bars of 1 standard deviation are included here and everywhere else.

point temperatures of concentrated aqueous salt solutions under confinement were reported to not exhibit concentration dependence.

The 210 K phase transition is absent for dilute solutions on either end of the phase diagram in Figure 2. Instead, the confined solutions appear to have composition-dependent melting points, which are inconsistent with the mass exchange between an external reservoir that has adopted the eutectic composition. Similar behavior has been previously reported for dilute NaCl aqueous solutions confined within MCM-41 and SBA-15 mesoporous silicas.[28] In this example, melting points of confined solutions depend on both solute concentration and pore size diameter. It is notable that fusion temperatures of dilute NaCl solutions confined within MCM-41 fall below the solidus temperature of the unconfined solution, suggesting that these solutions are unable to achieve the eutectic composition. $LiBF_4$ and $LiPF_6$ dimethyl carbonate solutions also experience concentration-dependent melting points when confined within MCM-41 and/or SBA-15 silicas, regardless of the presence or absence of an external reservoir.[29,30]

For dilute solutions, such as those encountered at high and low mole fractions of benzene in Figure 2, a substantial amount of solid phase will accumulate before the external reservoir freezes entirely. It is possible that the excessive amounts of solid material will block the pore openings, thereby preventing the confined solution from undergoing mass exchange with the unconfined solution. Furthermore, thermal scanning rates as well as the relative volumes of the external reservoir and the mesopores are two additional confounding variables that may play a role in facilitating mass exchange between confined and unconfined solutions during the freezing process. It should be stressed that all of these variables will likely affect the range of compositions over which the confined solution adopts the bulk eutectic composition.

Our SANS experiments focus on solutions having 0.80 mol fraction benzene because this composition is almost perfectly contrast matched to the silica pore walls when prepared with deuterated benzene and protonated cyclohexane. This composition is very close to the crossover point between composition-dependent and -independent melting point regions in Figure 2. However, as shown below, the experimentally observed DBDC and DBPC intensity ratios for the first and second Bragg peaks in the SANS data are inconsistent with the confined solution having the eutectic composition. Instead, the SANS data are better explained by a confined solution that retains the nominal 0.80 mol fraction benzene.

SANS of Confined Benzene and Cyclohexane Solutions. Small-angle neutron scattering is ideally suited for measuring ensemble-averaged morphologies with dimensions on the order of nanometers to submicrons. SANS probes the structure of our powder sample over all possible orientations in space. However, the measured intensity, $I(q)$, associated with the ordered pores dominates when the momentum transfer, $\vec{q}$, is equal to $2\pi/d$, where d_i is the spacing between planes of scattering centers and α (the angle between the cylinder long axis and $\vec{q}$, Figure 1d) is 90°. This scattering from periodically ordered lattice is referred to as the structure factor, $S(q)$, which gives rise to the two obvious delta functions (Bragg peaks) in Figure 3. The intensity of $S(q)$ is weighted by the form factor of individual cylinders, $F^2(q,D)$, discussed below. Additionally, a Porod[31] (or power law) scattering of form q^{-m} is observed when there is a contrast between the surrounding medium and objects of sufficiently large size such that $2\pi/\text{size} \ll q$. Here, this is attributed to the mesoporous silica grains in solution. Mathematically, the intensity is then expressed as[32,33]

$$I(q) \propto Pq^{-m} + \frac{V_F}{\nu}F^2(q, D)S(q) \quad (1)$$

$$F(q, D) = 2\nu\frac{\sin(qL/\sqrt{2})}{qL/\sqrt{2}}\left(\Delta\rho_{core}\left[\frac{J_1(qD_{core}/2)}{qD/2}\right] + \Delta\rho_{shell}\left[\frac{J_1(qD_{shell}/2)}{qD/2} - \frac{J_1(qD_{core}/2)}{qD/2}\right]\right) \quad (2)$$

P is the Porod scale factor and m is the exponent. F is the form factor for a core−shell cylinder[32,33] of respective core and shell diameters, D_{core} and D_{shell}, length L, cylinder volume ν, and sample volume fraction V_F. $\Delta\rho$ is the difference in ρ from the SiO_2 matrix. J_1 represents the first Bessel function. Instrumental smearing is calculated,[25,34] and these delta functions are broadened into two prominent Lorentzian-shaped peaks, labeled $Bragg_1$ and $Bragg_2$ in Figure 3.

DOI: 10.1021/acs.jpcc.7b11365
J. Phys. Chem. C 2018, 122, 7676−7684

ρ is a measure of how strongly a given material interacts with incident neutrons. By replacing naturally occurring, protonated cyclohexane (PC) with deuterated cyclohexane (DC), a markedly different ρ is obtained, as shown in Table 1. This

Table 1. Calculation of ρ as a Function of Miscible Material Compositions[a]

compound	composition	ρ at 303 K (10^{-6} Å^{-2})	ρ at 153 K (10^{-6} Å^{-2})
mesoporous silica	SiO_2	3.36	3.36
PC	C_6H_{12}	−0.279	−0.356
DC	C_6D_{12}	6.70	8.57
DB	C_6D_6	5.43	6.91
DBDC (nominal)	$0.80C_6D_6 + 0.20C_6D_{12}$	5.73	7.30
DBPC (nominal)	$0.80C_6D_6 + 0.20C_6H_{12}$	4.10	5.22
DBDC (eutectic)	$0.22C_6D_6 + 0.78C_6D_{12}$	N/A	8.26
DBPC (eutectic)	$0.22C_6D_6 + 0.78C_6H_{12}$	N/A	1.01

[a]The densities of PC, DC, and DB are 0.779, 0.893, and 0.950 g cm^{-3}, respectively, at 303 K and 0.996, 1.14, and 1.21 g cm^{-3}, respectively, at 153 K.

control of contrast greatly enhances sensitivity to the placement of cyclohexane within the pore structures, which is observed as a change in the intensity of $F^2(q,D)$ (eq 2) for q values located at Bragg peak positions.

The experimental scattering patterns obtained at 303 K (liquid phase) and 153 K (solid phase) are shown in Figure 3a,b. The solid curves correspond to the data fits in SasView[33] involving a Porod slope plus three Lorentzians of variable intensities located at 0.058, 0.112, and 0.180 Å^{-1} with full-width half-maximums of 0.0042, 0.015, and 0.050 Å^{-1}, respectively, which capture the essence of eqs 1 and 2. Including a contribution to the Lorentzian peak width beyond that of the instrumental smearing is an indication that there is some polydispersity in the pore-to-pore distance. The parameters of these fits are given in Table S1. For the 303 K solutions, a universal Porod exponent of m = 3.4 fits the data well. This value of m is quite reasonable for the mesoporous spheres because m = 4 corresponds to a perfectly smooth sphere, whereas m = 3 corresponds to a collapsed polymer coil.[31] At 153 K, the Porod exponent increases slightly to 3.38 for DB, 3.46 for DBDC, and 3.60 for DBPC. These increases in m could indicate the formation of interfaces between air and frozen solvent and/or the formation of cyclohexane-rich and benzene-rich frozen domains in the solution surrounding the mesoporous silica.

The open scattering is indistinguishable between 303 and 153 K, confirming that no measurable thermal contraction of SiO_2 occurs upon cooling. Thus, the intensities of the open Bragg peaks, denoted $I_{Bragg,open}$, are an ideal reference to which other data are compared. The relevant peak ratios of Table S1 are provided in Table 2, columns 1 and 2. $I(q) \propto \Delta\rho^2$ for open pores and pores containing solutions that are fully miscible. At 303 K, benzene and cyclohexane−benzene solutions meet these requirements, allowing for the determination of ρ for the mesoporous silica matrix. Using the calculated ρ's of DB and DBDC and matching the ratios of I_{Bragg_1} for DB and DBDC to open (Table 2), the best fit of ρ for SiO_2 was determined to be 3.36×10^{-6} Å^{-2}, which is only slightly less than the literature value for amorphous SiO_2 at 3.47×10^{-6} Å^{-2}.[35,36] Owing to near-contrast matching between SiO_2 and DCPC, which results in a low-intensity $Bragg_1$ peak at 303 K, the DBPC sample has been excluded from this fit. At 303 K, the close agreement between the calculated and experimental $\frac{I_{Bragg_1,solution}}{I_{Bragg_1,open}}$ ratios in Table 2, as well as a similarity in $Bragg_1$ and $Bragg_2$ ratios within ≈10% uncertainty, confirms that the solutions are miscible.

In contrast, at 153 K, the experimentally determined ratios of $\frac{I_{Bragg_1,DB}}{I_{Bragg_1,open}}$, $\frac{I_{Bragg_1,DBDC}}{I_{Bragg_1,open}}$, and $\frac{I_{Bragg_1,DBPC}}{I_{Bragg_1,open}}$ cannot be explained by uniform, miscible solutions, as listed in Table 2. Notably, the measured intensities of $\frac{I_{Bragg_1,DBDC}}{I_{Bragg_1,open}}$ and $\frac{I_{Bragg_1,DBPC}}{I_{Bragg_1,open}}$ at 153 K are 1.54 and 10.6 times larger than what is calculated for miscible solutions of the nominal composition, respectively. Although the eutectic composition could explain $\frac{I_{Bragg_1,DBDC}}{I_{Bragg_1,open}}$, it cannot explain $\frac{I_{Bragg_1,DBPC}}{I_{Bragg_1,open}}$. In fact, varying the composition of the miscible solutions from 0 to 100% of cyclohexane cannot explain the $\frac{I_{Bragg_1,DBDC}}{I_{Bragg_1,open}}$ and $\frac{I_{Bragg_1,DBPC}}{I_{Bragg_1,open}}$ experimentally measured ratios. Moreover, the statistically different $Bragg_1$ and $Bragg_2$ ratios per sample are a second indication that data cannot be explained by any miscible solution for which the Bragg peak ratios would be intrinsically the same (to be demonstrated next).

The simplest, nonmiscible morphology is that of a segregated core and shell running parallel to the cylinder-pore long axis (eq 2). Modeled $F^2(q,D)$ scattering from miscible, cyclohexane-corelbenzene-shell, and benzene-corelcyclohexane-shell mor-

Table 2. Experimental and Calculated $\frac{I_{solution}}{I_{open}} = \frac{(\rho_{solution} - \rho_{SiO_2})^2}{(\rho_{open} - \rho_{SiO_2})^2}$ Ratios, Where the Uncertainty on the Experimental Values is Less than 10%[a]

sample	experimental $Bragg_1$ ratio	experimental $Bragg_2$ ratio	calculated, nominal ratio	calculated, eutectic ratio
DB at 303 K	0.40	0.45	0.38	N/A
DBDC at 303 K	0.47	0.50	0.50	N/A
DBPC at 303 K	too small	too small	0.049	N/A
DB at 153 K	1.17	0.67	1.16	N/A
DBDC at 153 K	2.13	1.20	1.38	2.13
DBPC at 153 K	3.24	0.91	0.306	0.489

[a]Calculated values assume that SiO_2 $\rho = 3.36 \times 10^{-6}$ Å^{-2} and that the solutions are fully miscible, where miscible solutions intrinsically yield the same value for the $Bragg_1$ ratio and the $Bragg_2$ ratio.

DOI: 10.1021/acs.jpcc.7b11365
J. Phys. Chem. C 2018, 122, 7676−7684

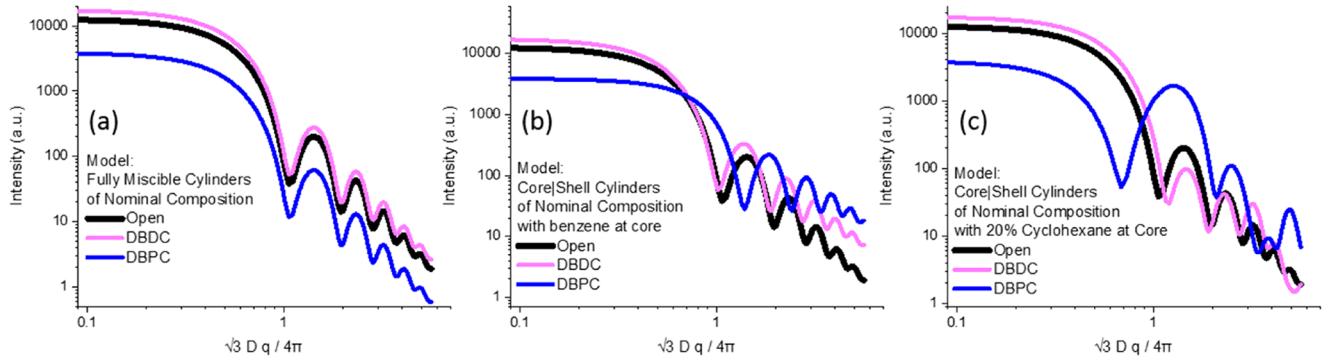

Figure 4. Simulated scattering for solutions of nominal composition at 153 K at several different possible morphologies.

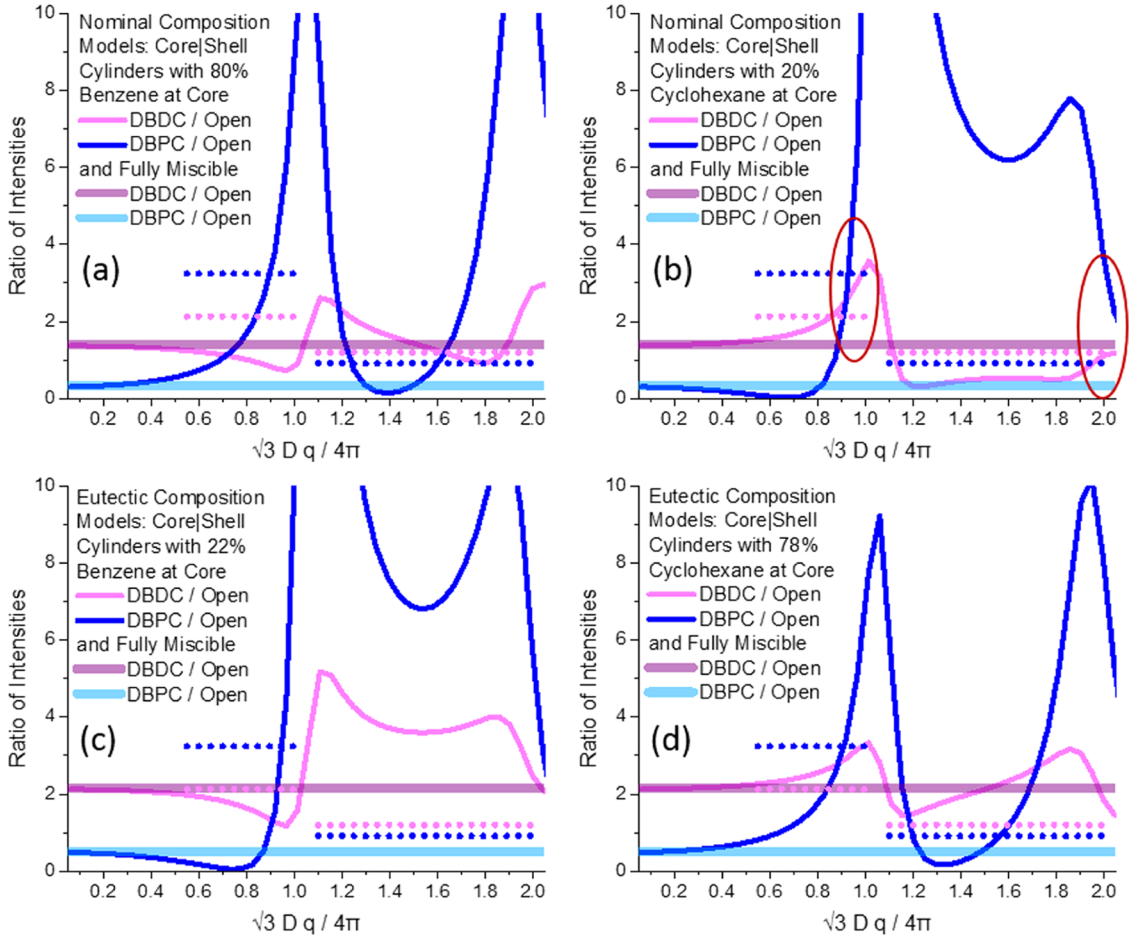

Figure 5. Simulated scattering ratios for solutions of nominal composition at 153 K of miscible, benzene-corelcyclohexane-shell, and cyclohexane-corelbenzene-shell morphologies. The dotted lines represent experimental data ratios, whereas the solid thick (flat) lines are the fully miscible models. The top and bottom rows correspond to nominal and eutectic solution compositions, respectively. The red circles indicate the best match among the models considered here, to be refined in subsequent text.

phologies are shown in Figure 4. Figure 5a,b provides the corresponding solution to open pore scattering ratios. The use of a generic diameter, D, with the multiplication of q by $\sqrt{3}D/4\pi$ is described below. The most obvious feature of Figures 4 and 5 is that miscible solutions produce ratios that are constant as a function of q (thick solid lines of Figure 5) and, thus, they cannot explain the differing Bragg_1 and Bragg_2 ratios per solution observed at 153 K.

In a hexagonally close-packed structure, Figure 1b, the lowest-q reflection peak would correspond to $4\pi/\sqrt{3}\kappa$, where κ is the pore center-to-pore center distance. The lowest-q reflection of 0.058 $Å^{-1}$ (or 0.057 $Å^{-1}$ from X-ray diffraction; Supporting Information) corresponds to κ = 12.5 nm. Owing to porosity of the SiO_2 matrix and likely widening of the pores away from the mesoporous silica surfaces, the exact outer pore diameter D ($=D_{\text{shell}}$) is unknown, but it must be ≥6.9 nm (see Figure 1b) and ≤12.5 nm (κ). This means that D could range from 0.55κ up to 1.0κ. However, altering D while keeping the ratio of core and shell volumes fixed simply stretches/compresses the scattering profile of $F^2(q,D)$ along q. Thus, an $F^2(q,D)$ model of generic D can be plotted against $\sqrt{3}Dq/4\pi$,

DOI: 10.1021/acs.jpcc.7b11365
J. Phys. Chem. C 2018, 122, 7676−7684

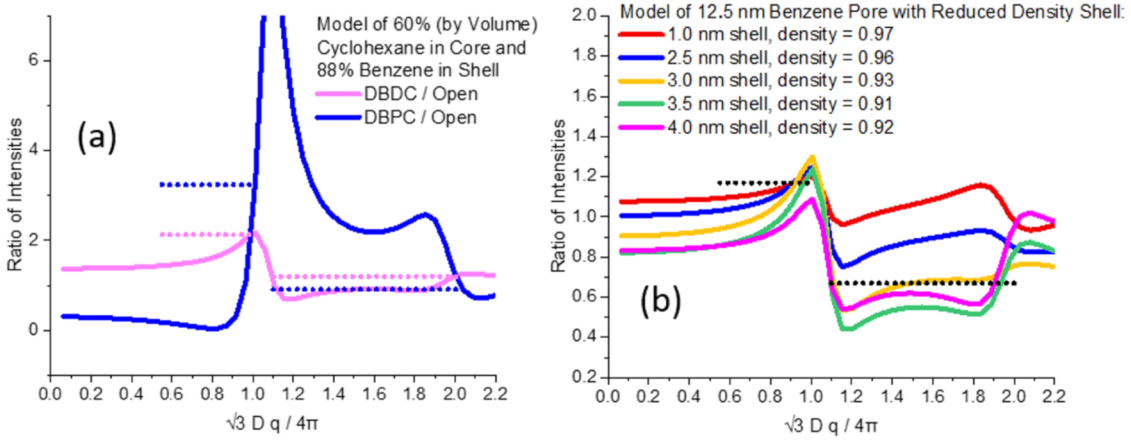

Figure 6. Best-fit models where dotted lines represent experimental Bragg peak ratios. (a) A cyclohexane-core|benzene-shell model at 153 K where solution exchange is allowed between the two regions. (b) Models of benzene at 153 K with reduced density shells, where a shell of 3.0−3.5 nm (1.75 nm of this shell within the porous SiO_2) yields the best fits.

where the desired ratios of $\frac{I_{\mathrm{Bragg_1,DBPC}}}{I_{\mathrm{Bragg_1,open}}} \geq 3.24$ and $\frac{I_{\mathrm{Bragg_1,DBDC}}}{I_{\mathrm{Bragg_1,open}}} \geq 2.13$ (Table 2) must simultaneously occur at a single value of $\sqrt{3Dq/4\pi}$ between 0.552 and 1.0. Additionally, the $\frac{I_{\mathrm{Bragg_2,DBPC}}}{I_{\mathrm{Bragg_2,open}}} \geq 0.91$ and $\frac{I_{\mathrm{Bragg_2,DBDC}}}{I_{\mathrm{Bragg_2,open}}} \geq 1.20$ (Table 2) must also occur at a single q-value of $\sqrt{3Dq/4\pi}$ between 1.1 and 2.0, which is approximately twice that of the first Bragg peak. These requirements are shown as dotted lines in Figures 5 and 6. Note that ratios slightly different from the experimentally observed ones can be valid because mixing of the cyclohexane and benzene or a graded interface between the core and shell tends to push the observed scattering closer toward the fully miscible case (solid thick lines of Figure 5).

Figure 5 shows the modeled $F^2(q,D)$ scattering ratios at 153 K for a variety of possible conditions: miscible solutions of nominal or eutectic composition (thick lines), core|shell segregation of solutions of nominal or eutectic composition with the benzene located at the core (column 1), and core|shell segregation of solutions of nominal or eutectic composition with the cyclohexane located at the core (column 2). Neither nominal nor eutectic compositions of miscible solutions (thick lines of Figure 5) come close to reproducing the dotted lines required for the $Bragg_1$ or $Bragg_2$ ratios. The nominal and eutectic solutions with the benzene concentrated toward the pore centers also do not reproduce the dotted line requirements, as shown in Figure 5a,c. However, concentrating the cyclohexane at the pore center, as shown in Figure 5b,d can explain the experimental data. A significantly better match to both the $Bragg_1$ and $Bragg_2$ peak ratios is found for the solutions of nominal composition (Figure 5b, red circles) than that of the eutectic composition (Figure 5d) because the eutectic $Bragg_2$ ratios cannot meet the experimental, dotted line values even with unlimited core and shell mixing.

Some diffusion or gradient between the cyclohexane and benzene core|shell morphology is expected. Although there are many possible variations in modeling the boundary "fuzziness", here a simple model is used that retains the core|shell boundary radius associated with a segregated 20% mol fraction cyclohexane and 80% mol fraction benzene solution (23.3% cyclohexane and 76.7% benzene by volume), yet the model allows a fraction of the cyclohexane and benzene in the core and shell regions within the pores to exchange while preserving the nominal composition within the entire pore. Setting the core to be 60% cyclohexane and 40% benzene by volume, the shell becomes 88% benzene and 12% cyclohexane by volume, as shown in Figure 6a. Because the DSC data clearly indicate a first-order phase transition, the formation of a glassy solid is ruled out. Instead, the SANS and DSC data are consistent with the formation of benzene and cyclohexane crystallites in the interior of the pores. This is consistent with wide-angle neutron scattering experiments that show crystallization of benzene when confined within SBA-15 silica at 70 K.[17]

Here, both $Bragg_1$ and $Bragg_2$ ratios are achieved for the DBDC and DBPC near $\sqrt{3qD/4\pi} = 1$ and 2, respectively. Other modeling variations of a graded surface also consistently require D to be close to κ, which implies either that the internal pore diameters widen to near 12.5 nm deep within the silica grains or that the silica in the pore walls is also highly porous (consistent with the Hg porisometry results). Indeed, modeling reveals that porous silica volume fractions up to 25% (see the Supporting Information) can explain the data well; this is consistent with SBA-15[37,38] and MSU-H[39] silicas, where individual pores are believed to be interconnected with smaller nanopores. The key to a successful model is that the cyclohexane must be preferentially phase segregated toward the pore centers at 153 K.

SANS of Confined Benzene. Finally, evaluation of a single component sample, containing only deuterated benzene, is of relevance in that it provides insight between competing models regarding the benzene distribution along the silica interface. Although Xia et al.[17] proposed a uniform increase in the density of confined benzene throughout the pores, there is a class of models that suggests benzene may form a shell that differs in density from the core, but these models yield seemingly disparate thicknesses. Sub-nanometer shells have been proposed on the premise that benzene molecules could orient parallel to the silica surface, enabling strong Coulombic interactions between π electrons of benzene and the polar silica surface.[9] This idea is supported by NMR spectroscopy at 168 K,[17] molecular dynamic simulations,[9] and Raman and optical Kerr effect spectra,[7] which suggest a localized shell 0.2−0.5 nm thick. Yet, ^{2}H NMR spectroscopy of deuterated benzene confined within SBA-15 at 110 and 120 K places the benzene shell thickness at 2.45 nm,[10] whereas ^{2}H NMR spectra

DOI: 10.1021/acs.jpcc.7b11365
J. Phys. Chem. C 2018, 122, 7676−7684

of deuterated benzene confined inside porous-glass mesocellular foam over the temperature range of 90−180 K yield a shell thickness of 1.65 nm thickness.[18] Additionally, DSC studies of confined cyclohexane place the thickness of the nonfreezable surface layer at 2.14 nm.[8]

The SANS frozen benzene data also support a corelshell model of varied density given that the $Bragg_1$ and $Bragg_2$ ratios are measurably different at 153 K; see Table 2. Note that it can be mathematically proven from eqs 1 and 2 that the difference in solution density is not correlated with the presence of the porous silica, but rather this is a measure of the intrinsic benzene density as a function of radius. Moreover, in liquid form at 303 K, the Bragg peak ratios are equivalent within error bars. Our SANS data are best fit by thicker 3.5 nm shell models (for D = 12.5 nm) with a reduction in density to about 91% of the bulk; see Figure 6b. Other combinations of shell thickness and density shown in Figure 6b either fail to match the experimental intensity ratios for $Bragg_1$ and $Bragg_2$ or give incorrect ratios of $\sqrt{3}Dq/4\pi$ for the two Bragg peaks at the desired intensity ratio. Assuming that the pore diameter is 9 nm from the N_2 physisorption measurements, this places the interfacial layer thickness at ≈1.8 nm along the SiO_2 walls, with the remaining interfacial benzene penetrating deep into the voids and nanoporous tunnels that inhabit the walls. However, if the pore diameter is taken to be 6.9 nm based on TEM measurements (Figure 1b), this would place the interfacial layer thickness at only ≈0.7 nm along the SiO_2 walls. It is possible that the conflicting reports of shell thickness could in part reflect the extent to which different experimental techniques account for leakage into the surrounding medium.

CONCLUSIONS

It is shown here that binary solutions of 0.80 mol fraction benzene and 0.20 mol fraction cyclohexane confined within 9.0 nm SiO_2 pores are fully miscible at 303 K, yet they clearly phase segregate below their component freezing points at 153 K. Moreover, the cyclohexane molecules preferentially segregate toward the center of the pores upon freezing, as revealed by enhanced SANS sensitivity to its placement using selective deuteration/protonation of the cyclohexane. Because neither cyclohexane nor benzene chemically bonds with SiO_2, this segregation appears to be driven primarily by confinement. The data also indicate that upon cooling to 153 K, pure benzene becomes less dense within both the porous SiO_2 and a subnanometer interfacial region located along the pore surface, whereas its core forms a solid phase consistent with an unconfined solution.

ASSOCIATED CONTENT

Supporting Information

The Supporting Information is available free of charge on the ACS Publications website at DOI: 10.1021/acs.jpcc.7b11365.

Additional experimental details concerning DSC, TEM, N_2 physisorption, Hg porisometry, and X-ray diffraction analysis of the mesoporous silica; details of the SANS fits and the effect of pore wall porosity on the models (PDF)

AUTHOR INFORMATION

Corresponding Authors

*E-mail: kathryn.krycka@nist.gov (K.L.K.).
*E-mail: burba@nsuok.edu (C.M.B.).

ORCID

Kathryn L. Krycka: 0000-0002-6393-3268
Christopher M. Burba: 0000-0001-9503-0664

Notes

The authors declare no competing financial interest.

ACKNOWLEDGMENTS

C.M.B. and L.J.L. are grateful to the Oklahoma Louis Stokes Alliance for Minority Participation (NSF HRD 1408748) for providing travel support. Access to NGB 30 m SANS was provided by the Center for High Resolution Neutron Scattering, a partnership between the National Institute of Standards and Technology and the National Science Foundation under Agreement No. DMR-1508249.

REFERENCES

(1) Schreiber, A.; Ingke, K.; Findenegg, G. H. Melting and Freezing of Water in Ordered Mesoporous Silica Materials. *Phys. Chem. Chem. Phys.* **2001**, *3*, 1185−1195.
(2) Tombari, E.; Salvetti, G.; Ferrari, C.; Johari, G. P. Thermodynamic Functions of Water and Ice Confined to 2 nm Radius Pores. *J. Chem. Phys.* **2005**, *122*, No. 104712.
(3) Kittaka, S.; Ishimaru, S.; Kuranishi, M.; Matsuda, T.; Yamaguchi, T. Enthalpy and Interfacial Free Energy Changes of Water Capillary Condensed in Mesoporous Silica, MCM-41 and SBA-15. *Phys. Chem. Chem. Phys.* **2006**, *8*, 3223−3231.
(4) Dutta, D. P.; Sharma, S. K.; Maheshwari, P.; Sudarshan, K.; Pujari, P. K. Freezing of Nanodroplets: Phase Transition of Organic Liquids Confined in Nanopores Studied by Positron Annihilation Spectroscopy. *Mater. Sci. Forum* **2009**, *607*, 218−222.
(5) Dosseh, G.; Xia, Y.; Alba-Simionesco, C. Cyclohexane and Benzene Confined in MCM-41 and SBA-15: Confinement Effects on Freezing and Melting. *J. Phys. Chem. B* **2003**, *107*, 6445−6453.
(6) Dutta, D.; Pujari, P. K.; Sudarshan, K.; Sharma, S. K. Effect of Confinement on the Phase Transition of Benzene in Nanoporous Silica: A Positron Annihilation Study. *J. Phys. Chem. C* **2008**, *112*, 19055−19060.
(7) Zhu, X.; Farrer, R. A.; Fourkas, J. T. Ultrafast Orientational Dynamics of Nanoconfined Benzene. *J. Phys. Chem. B* **2005**, *109*, 12724−12730.
(8) Amanuel, S.; Bauer, H.; Bonventre, P.; Lasher, D. Nonfreezing Interfacial Layers of Cyclohexane in Nanoporous Silica. *J. Phys. Chem. C* **2009**, *113*, 18983−18986.
(9) Coasne, B.; Fourkas, J. T. Structure and Dynamics of Benzene Confined in Silica Nanopores. *J. Phys. Chem. C* **2011**, *115*, 15471−15479.
(10) Gedat, E.; Schreiber, A.; Albrecht, J.; Emmler, T.; Shenderovich, I.; Findenegg, G. H.; Limbach, H.-H.; Buntkowsky, G. 2 H-Solid-State NMR Study of Benzene-D 6 Confined in Mesoporous Silica SBA-15. *J. Phys. Chem. B* **2002**, *106*, 1977−1984.
(11) Scatchard, G.; Wood, S. E.; Mochel, J. M. Vapor-Liquid Equilibrium. III. Benzene-Cyclohexane Mixtures. *J. Phys. Chem.* **1939**, *43*, 119−130.
(12) Rastogi, R. P.; Nigam, R. K. Thermodynamic Properties of Binary Mixtures of Benzene, Cyclohexane and Carbon Tetrachloride. *Trans. Faraday Soc.* **1959**, *55*, 2005−2012.
(13) Shao, Y.; Hoang, G.; Zerda, T. W. Solid-Solid Phase Transitions of Cyclohexane in Porous Sol-Gel Glass. *J. Non-Cryst. Solids* **1995**, *182*, 309−314.
(14) Dore, J.; Webber, B.; Strange, J.; Farman, H.; Descamps, M.; Carpentier, L. Phase Transformations for Cyclohexane in Mesoporous Silicas. *Phys. A* **2004**, *333*, 10−16.
(15) Mu, R.; Malhotra, V. M. Effects of Surface and Physical Confinement on the Phase Transitions of Cyclohexane in Porous Silica. *Phys. Rev. B* **1991**, *44*, 4296−4303.

DOI: 10.1021/acs.jpcc.7b11365
J. Phys. Chem. C 2018, 122, 7676−7684

(16) Qing, Y.; Zenan, Z.; Deyu, K.; Rongshen, C. Interfacial Contact Angle Measurements of Water, Mercury, Organic Liquids on Quartz, Calcite, Montmorillonite. *Constr. Build. Mater.* **2007**, *21*, 539−545.
(17) Xia, Y.; Dosseh, G.; Morineau, D.; Alba-Simionesco, C. Phase Diagram and Glass Transition of Confined Benzene. *J. Phys. Chem. B* **2006**, *110*, 19735−19744.
(18) Masierak, W.; Emmler, T.; Gedat, E.; Schreiber, A.; Findenegg, G. H.; Buntkowsky, G. Microcrystallization of Benzene-d6 in Mesoporous Silica Revealed by 2H Solid-State Nuclear Magnetic Resonance. *J. Phys. Chem. B* **2004**, 18890−18896.
(19) Eberle, A. P.; King, H. E.; Ravikovitch, P. I.; Walters, C. C.; Rother, G.; Wesolowski, D. J. Direct Measure of the Dense Methane Phase in Gas Shale Organic Porosity by Neutron Scattering. *Energy Fuels* **2016**, *30*, 9022−9027.
(20) Ramsay, J. D. F.; Hoinkis, E. SANS Investigations of Benzene Adsorption on Porous Silica Gel. *Phys. B* **1998**, *248*, 322−326.
(21) Lin, M. Y.; Sinha, S. K.; Drake, J. M.; Wu, X. L.; Thiyagarajan, P.; Stanley, H. B. Study of Phase Separation of a Binary Fluid Mixture in Confined Geometry. *Phys. Rev. Lett.* **1994**, *72*, 2207.
(22) Hellweg, T.; Schemmel, S.; Rother, G.; Brûlet, A.; Eckerlebe, H.; Findenegg, G. H. De-Mixing Dynamics of a Binary Liquid System in a Controlled-Pore Glass. *Eur. Phys. J. E: Soft Matter Biol. Phys.* **2003**, *12*, 1−4.
(23) Schemmel, S.; Rother, G.; Eckerlebe, H.; Findenegg, G. H. Local Structure of a Phase-Separating Binary Mixture in a Mesoporous Glass Matrix Studied by Small-Angle Neutron Scattering. *J. Chem. Phys.* **2005**, *122*, No. 244718.
(24) Abdel Hamid, A. R.; Mhanna, R.; Lefort, R.; Ghoufi, A.; Alba-Simionesco, C.; Frick, B.; Morineau, D. Microphase Separation of Binary Liquids Confined in Cylindrical Pores. *J. Phys. Chem. C* **2016**, *120*, 9245−9252.
(25) Kline, S. R. Reduction and Analysis of SANS and USANS Data Using Igor Pro. *J. Appl. Crystallogr.* **2006**, *39*, 895−900.
(26) Jackson, C. L.; McKenna, G. B. The Melting Behavior of Organic Materials Confined in Porous Solids. *J. Chem. Phys.* **1990**, *93*, 9002−9011.
(27) Meissner, J.; Prause, A.; Findenegg, G. H. Secondary Confinement of Water Observed in Eutectic Melting of Aqueous Salt Systems in Nanopores. *J. Phys. Chem. Lett.* **2016**, *7*, 1816−1820.
(28) Burba, C. M.; Janzen, J. Confinement Effects on the Phase Transition Temperature of Aqueous NaCl Solutions: The Extended Gibbs-Thomson Equation. *Thermochim. Acta* **2015**, *615*, 81−87.
(29) Butson, E.; Atchley, J.; Burba, C. M. Confinement Effects on the Thermal and Conductivity Properties of $LiPF_6$-Dimethyl Carbonate Solutions Relevant to Lithium Rechargeable Batteries. *ECS Trans.* **2011**, *35*, 77−85.
(30) Burba, C. M.; Butson, E. D.; Atchley, J. R.; Johnson, M. S. Thermal Properties and Ionic Conductivities of Confined LiBF4 Dimethyl Carbonate Solutions. *J. Phys. Chem. C* **2014**, *118*, 366−375.
(31) Sivia, D. S. *Elementary Scattering Theory For X-Ray and Neutron Users*; Oxford University Press: Oxford, 2011.
(32) Guinier, A. G.; Fournet, G. *Small-Angle Scattering of X-Rays*; John Wiley and Sons: New York, 1955.
(33) SASView software can be found at sasview.org.
(34) Mildner, D. F. R.; Barker, J. G.; Kline, S. R. The Effect of Gravity on the Resolution of Small-Angle Neutron Diffraction Peaks. *J. Appl. Crystallogr.* **2011**, *44*, 1127−1129.
(35) Haynes, W. M. *CRC Handbook of Chemistry and Physics*, 92nd ed.; CRC Press: Boca Raton, FL, 2011.
(36) Dianoux, A.-J.; Lander, G. *Neutron Data Booklet*, 2nd ed.; Institut Laue-Langevin: Grenoble, France, 2003.
(37) Galarneau, A.; Cambon, H.; Di Renzo, F.; Ryoo, R.; Choi, M.; Fajula, F. Microporosity and Connections between Pores in SBA-15 Mesostructured Silicas as a Function of the Temperature of Synthesis. *New J. Chem.* **2003**, *27*, 73−79.
(38) Ryoo, R.; Ko, C. H.; Kruk, M.; Antochshuk, V.; Jaroniec, M. Block-Copolymer-Templated Ordered Mesoporous Silica: Array of Uniform Mesopores or Mesopore−Micropore Network? *J. Phys. Chem. B* **2000**, *104*, 11465−11471.
(39) Kim, S. S.; Karkamkar, A.; Pinnavaia, T. J.; Kruk, M.; Jaroniec, M. Synthesis and Characterization of Ordered, Very Large Pore MSU-H Silicas Assembled from Water-Soluble Silicates. *J. Phys. Chem. B* **2001**, *105*, 7663−7670.

DOI: 10.1021/acs.jpcc.7b11365
J. Phys. Chem. C 2018, 122, 7676−7684